Viscoelastic Properties of Aligned Block Copolymer Lamellae

Hyeok Hahn, Joon H. Lee, and Nitash P. Balsara*

Department of Chemical Engineering, University of California, Berkeley, California 94720, and Materials Science Division, Lawerence Berkeley National Laboratory, Berkeley, California 94720

Bruce A. Garetz

Department of Chemical Engineering and Chemistry, Polytechnic University, Six Metrotech Center, Brooklyn, New York 11201

Hiroshi Watanabe*

Institute for Chemical Research, Kyoto University, Uji, Kyoto 611, Japan

Received June 8, 2001; Revised Manuscript Received September 7, 2001

ABSTRACT: Structure−property relationships of aligned block copolymer lamellae in the vicinity of the order−disorder transition are studied by a combination of optical birefringence and rheology. Minimizing defect density was a crucial part of our experiments. The organization of block copolymer chains into aligned lamellae leads to a reduction in both zero shear viscosity and compliance relative to the disordered state. The frequency dependencies of the storage and loss shear moduli of the aligned lamellae are close to the Rouse prediction. In addition, the measured value of the compliance of the ordered and aligned state is within a factor of 2 of the Rouse prediction (agreement obtained with no adjustable parameters). In contrast, large differences between the experiments and the Rouse model are seen in the disordered state due to the presence of concentration fluctuations.

Introduction

Despite considerable effort, the molecular origins of the measured rheological properties of lamellar block copolymers have not been fully established.[1−32] Samples made in the absence of external fields consist of randomly oriented grains with concomitant point, line, wall, and continuous (texture) defects.[31,32] The application of appropriate shear flow results in the elimination of defects, and the lamellar planes are aligned in the flow direction.[1,5,10,11,14,15,18,19−31] Two kinds of flow aligned states are usually reported: the parallel alignment wherein lamellae lie parallel to the shear plates, and the perpendicular alignment wherein the lamellae lie perpendicular to the shear plates. Understanding the rheological properties of these aligned states is a necessary first step for understanding the rheology of defect-filled samples.

The rheological properties of aligned block copolymer lamellae are highly anisotropic due to their smectic liquid crystalline character.[25,26,33−39] The rheology of small molecule smectic phases is dominated by viscous dissipation and thus characterized by Leslie viscosities. In contrast, the rheology of smectic phases formed by polymer molecules will contain additional contributions due to the elastic response of the polymer chains. The parameter that characterizes the elastic features of a system in the long time limit is the compliance.[40,41] Complete rheological characterization of aligned block copolymer lamellae thus requires specification of both viscosity and compliance.

Both parallel and perpendicular aligned states of any smectic liquid crystal must exhibit terminal behavior:[33−39] the frequency (ω) dependence of the storage and loss moduli, G' and G'', respectively, must obey the power laws $G' \sim \omega^2$ and $G'' \sim \omega^1$ as $\omega \rightarrow 0$. The zero shear viscosity and compliance are defined by[40,41] $\eta_0 = [G''/\omega]_{\omega\rightarrow 0}$ and $J_0 = [G'/(G''^2)]_{\omega\rightarrow 0}$. However, most of the experimental rheological data of aligned block copolymer lamellae show nonterminal behavior,[20−27] thus precluding the determination of η_0 and J_0.

In this paper we study the rheological properties of aligned block copolymer lamellae. We present measurements of η_0 and J_0 and show that the organization of block copolymers into aligned lamellae leads to a reduction in both η_0 and J_0, relative to the disordered state. The reason for the reduction is discussed below.

Materials

A polystyrene−polyisoprene (SI) block copolymer was synthesized and characterized by methods described in ref 42. The weight-averaged molecular weights of both blocks were 34×10^3 g/mol, and we refer to the polymer as SI[34−34]. The ratio of the weight- to number-averaged molecular weights (M_w/M_n) was estimated by gel permeation chromatography to be 1.05. A 32.4 wt % solution of SI[34−34] in dioctylphthalate (DOP) was prepared using methods described in ref 43. The polymer chains in our system are essentially unentangled due to the relatively low SI molecular weight and concentration.[41] The order−disorder transition temperature (T_{ODT}) of the solution was determined to be 30 ± 1 °C using the birefringence method.[43] The average interlamellar spacing, determined by small-angle neutron scattering, was 33 nm.

Our sample was extremely fluid at room temperature (i.e., in the ordered state) and took the shape of the container in about 30 min. This is an indication that the relaxation processes in our ordered sample occur on relatively short time scales.[44] Our sample is thus ideally suited for low-frequency rheological studies.

Aliquots of the SI[34−34]/DOP solution were subjected to several optical and rheological experiments to ensure reproducibility. For brevity, we show results obtained from one set of experiments. To ensure a uniform initial condition, the samples were disordered by heating to 44 °C, prior to all of the experiments.

10.1021/ma0109929 CCC: $20.00
Published on Web 11/06/2001

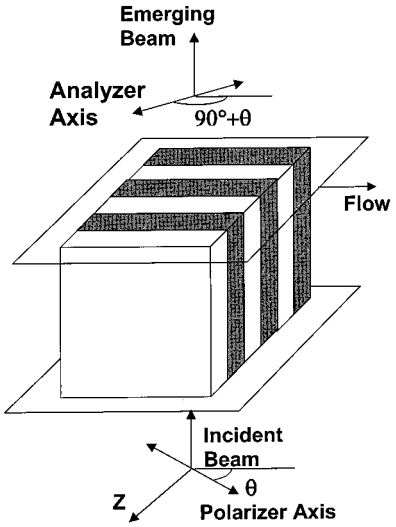

Figure 1. Schematic view of birefringence experiment showing lamellae in the perpendicular alignment. The angle between the polarization direction of the incident beam and the flow direction is θ.

Optical Characterization

The optical experiments were performed on an apparatus described in ref 45. The SI[34−34]/DOP sample with thickness $L = 2.0$ mm was held between two parallel quartz plates fitted into thermostated aluminum plates. The top plate was translated using a computer-controlled motor such that the time dependence of the displacement had a triangular waveform with an angular frequency ω_{optic}. The apparatus is shown schematically in Figure 1. The sample was illuminated by a polarized beam of light from a HeNe laser with wavelength (λ) of 0.632 μm (beam width was 1 mm). The fraction of incident light power transmitted through the sample in cross-polarized configuration with the incident beam polarized at an angle of θ to the flow direction, p, was measured as shown in Figure 1.

The sample was disordered at 44 °C and quenched to 22 °C. Time zero is defined as the time at which the set point on the temperature controller was changed. It took about 20 min for the sample temperature to reach within 1 °C of the target temperature. Reciprocating shear flow with frequency $\omega_{optic} = 0.8$ rad/s and a strain amplitude of 100% was imposed at $t = 0$. The time dependence of $p(\theta=45°)$ is represented by circles in Figure 2. The signal in the disordered state is small: $p(\theta=45°) \approx 10^{-4}$. We consider this to be background noise. The signal stays in the vicinity of 10^{-4} until $t =$ 80 min, rises rapidly by 3 orders of magnitude between $t = 80$ and $t = 200$ min, and levels off at 10^{-1} (Figure 2). The increase in $p(\theta=45°)$ indicates the formation of ordered grains that are comparable in size to the wavelength of light.[45−49] The plateau in the time dependence of $p(\theta=45°)$ indicates completion of order formation. Order formation under reciprocating shear flow is thus complete at $t \approx 200$ min.

In the second experiment, we studied order formation in our SI/DOP solution with the motor turned off; the thermal history was identical to that described above. The time dependence of $p(\theta=45°)$ obtained under quiescent conditions is represented by the squares in Figure 2. (In the absence of shear flow, the sample was isotropic, and thus p was independent of θ.[47]) It is evident from Figure 2 that the time dependencies of p obtained under quiescent conditions and oscillatory shear flow are similar: an initial value of p of 10^{-4}, followed by a rapid increase in p until $t \approx 200$ min, followed by a plateau. The time required for order formation under reciprocating flow and quiescent conditions is similar. Previous experiments using in-situ small-angle neutron scattering under shear flow led to the same conclusion.[49] It is clear from Figure 2 that the main effect of shear flow is on the magnitude of the plateau value of p. In the absence of shear flow p plateaus at 2×10^{-3} while in the presence of shear flow p plateaus at 10^{-1}.

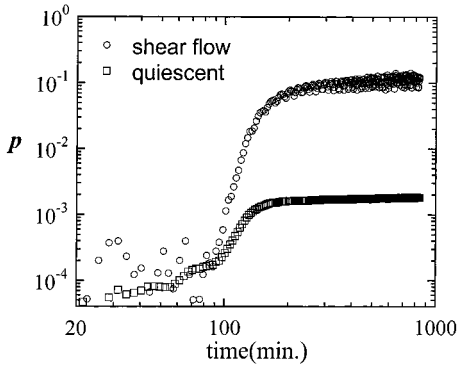

Figure 2. Time dependence of p, the fraction of incident light power transmitted through the sample in cross-polarized configuration with incident beam polarized at $\theta = 45°$ to the flow direction, from lamellae formed under shear flow (circles) and under quiescent condition (squares). The data are shown for $t \geq 20$ min (after thermal equilibration).

We have established that the signal from a collection of randomly oriented grains, obtained in the absence of external fields, is proportional to the average grain size.[47] If shear flow had caused parallel alignment of some fraction of the lamellar grains and elimination of some of the defects, it is straightforward to show that p of the aligned state would be lower than p obtained from sample composed of randomly oriented grains. On the other hand, a large increase in p is expected if all the lamellae are aligned in the perpendicular orientation.[45,47] In our system, we see that $p(\theta=45°)$ in the aligned state is about 2 orders of magnitude larger than that obtained from random grains. The data in Figure 2 thus unambiguously indicate the formation of perpendicular lamellae under the specified flow field.

After completing the alignment protocol described above (Figure 2), we stopped the shear flow and measured the angular (θ) dependence of p by manually rotating the crossed polarizers (see Figure 1). The theoretical expression for $p(\theta)$ of perpendicular lamellae shown in Figure 1 is

$$p(\theta) = \sin^2(2\theta) \sin^2(\pi|\Delta n|L/\lambda) \qquad (1)$$

where Δn is the difference between the refractive indices for light polarized parallel and perpendicular to the lamellar normal.[50]

The experimentally determined $p(\theta)$ at 22 °C is represented by filled circles in Figure 3. We then heated the sample under quiescent conditions in a stepwise manner, waiting for 50 min at each temperature to ensure thermal equilibration, and obtained $p(\theta)$ as a function of temperature (Figure 3). The curves through each data set are least-squares fits of eq 1 with $|\Delta n|$ as the only adjustable parameter. The fitting procedure thus yields the temperature dependence of $|\Delta n|$. If the polystyrene concentration in the z direction in Figure 1

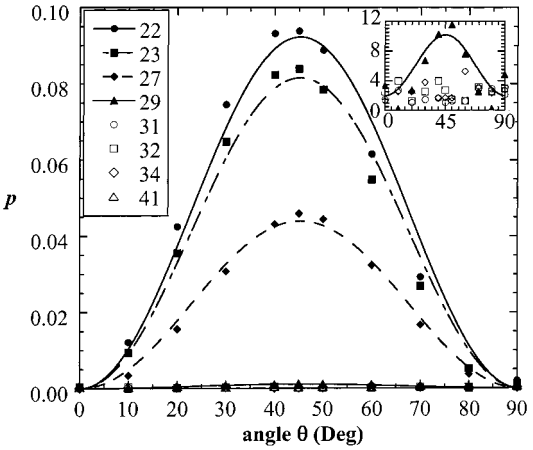

Figure 3. Plot of $p(\theta)$, the incident beam polarized at an angle of θ to the flow direction, at various temperatures. The curves are theoretical fits using eq 1 with Δn as the only adjustable parameter. Inset: $p(\theta) \times 10^4$ vs θ at $T \geq 29$ °C.

Table 1. Temperature Dependence of the Relative Order Parameter *A* for the SI/DOP Sample in the Ordered State

temperature (°C)	relative order parameter (A)
22	1.00
24	0.97
27	0.82
29	0.33

varies sinusoidally, as is assumed in weak segregation theories,[51,52] then the amplitude of the sine wave—or the order parameter—is proportional to $|\Delta n|^{1/2}$. We define the relative order parameter $A(T) = [(|\Delta n| \text{ at } T)/(|\Delta n| \text{ at } 22\ °C)]^{1/2}$. The value of A is the amplitude of the sine wave at a given temperature T relative to its value at 22 °C. The characteristic $\sin^2(2\theta)$ dependence of $p(\theta)$ is lost at temperatures ≥31 °C (see Figure 3). We conclude that $A = 0$ at temperatures ≥31 °C, and the average signal in this regime (2×10^{-4} units) was taken as a measure of background noise. The fitting of the $p(\theta)$ data was done after subtraction of the background noise; only the 29 °C data are affected by the background signal (see inset in Figure 3). The temperature dependence of A in the ordered state is given in Table 1.

Our optical characterization method is similar to that of Keller et al.[1,2] and Kornfield et al.[21−24] The consistency between information obtained by the optical method and that obtained by other methods such as small-angle X-ray and neutron scattering has been demonstrated in these papers.[1,2,21−24]

Rheology

We now discuss the rheological properties of our SI-[34−34]/DOP solution. Rheological measurements were performed using an ARES, rheometer from Rheometric Scientific Inc., with 25 mm parallel steel plates and 1 mm thick sample. The sample was deformed by rotating the lower plate; the time dependence of the displacement had a sinusoidal waveform with angular frequency ω. The sample was sheared after quenching from the disordered state (42 °C) to 22 °C (the time required to equilibrate the sample temperature after the changing the set temperature from 42 to 22 °C was 5 min) with $\omega = 1.0$ rad/s and an average strain amplitude of 100%.

The time dependence of the stress recorded during the shear alignment protocol ($t > 5$ min, the time required for thermal equilibration) is depicted in Figure 4. The peak value of the periodic, time-dependent stress during shear alignment σ_{peak} is shown in Figure 4. Our SI[34−34]/DOP solution exhibits nonmonotonic time dependence σ_{peak} (see Figure 4). We find a rapid increase in σ_{peak} until $t = 10$ min followed by a monotonic decrease in σ_{peak}. The stress decreases during most of the shear alignment process (10 min < t < 1000 min). The reason for the observed time dependence of σ_{peak} will be clarified later.

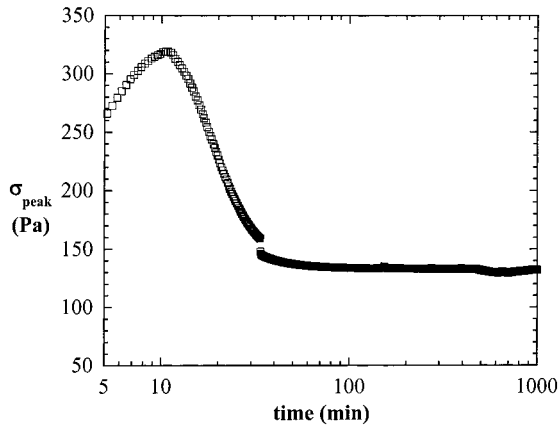

Figure 4. Time dependence of peak stress (σ_{peak}) during shear alignment process at 22 °C. The strain amplitude was 100%. The data are shown for $t \geq 5$ min (after thermal equilibration).

The alignment process in the rheometer was stopped at selected times, and dynamic storage and loss moduli, $G'(\omega)$ and $G''(\omega)$, respectively, were measured using 2% strain amplitude. Separate experiments indicated that this amplitude was small enough to detect linear viscoelastic response in our frequency window.

Figure 5 shows the $G'(\omega)$ and $G''(\omega)$ data obtained during the shear alignment process at 22 °C (in the ordered state). It is evident that G'' approaches a steady state in our frequency window after 300 min of alignment. In contrast, G' decreases continuously during the alignment process (for 660 min). This difference reflects different sensitivities of G' and G'' to slow relaxation modes.

Block copolymers exhibit fast and slow relaxation modes; the former corresponds to motion of individual copolymer chains while the latter corresponds to motion involving collections of chains.[53] In the ordered state, the slow relaxation modes could be characteristic of lamellae or grains or intergrain defects. In the disordered state, slow relaxation modes can arise due to the presence of concentration fluctuations.[19,53−55] Separating the relaxation spectrum of our system [$H(\tau)$] into fast [$H_{fast}(\tau)$] and slow [$H_{slow}(\tau)$] modes enables the expression of the corresponding components of the moduli as[41,53]

$$G'_{\xi}(\omega) = \omega^2 \int_{-\infty}^{\infty} \tau^2 H_{\xi}(\tau) \frac{1}{1+\omega^2\tau^2} \, d \ln \tau \quad (\xi = \text{fast, slow}) \quad (2)$$

$$G''_{\xi}(\omega) = \omega \int_{-\infty}^{\infty} \tau H_{\xi}(\tau) \frac{1}{1+\omega^2\tau^2} \, d \ln \tau \quad (\xi = \text{fast, slow}) \quad (3)$$

This expression provides the basis for understanding why G' ($=G'_{fast} + G'_{slow}$) changes during the final stages of alignment while G'' ($=G''_{fast} + G''_{slow}$) does not (Figure 5). Since H in the kernel for G'' is magnified by the first power of τ (eq 3), G'' is dominated by the fast modes

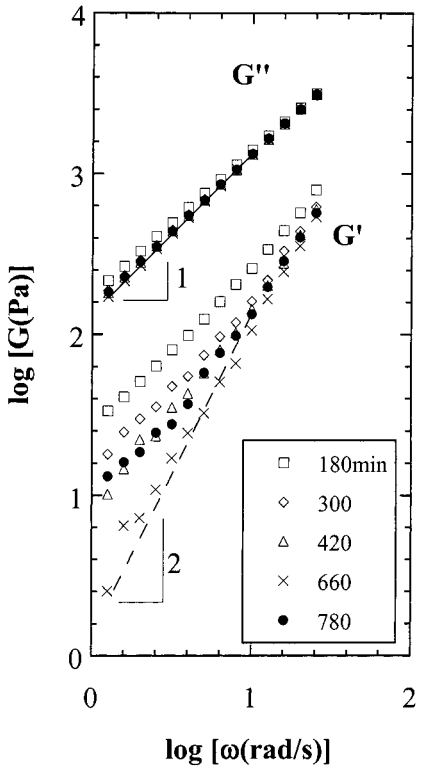

Figure 5. Frequency (ω) dependence of the storage (G') and loss (G'') moduli at selected times during the shear alignment process. Solid symbols show data obtained after holding the sample quiescently for 120 min after the shear alignment process, which lasted to 660 min, was completed. The lines were used to evaluate zero shear viscosity (η_0) and recoverable compliance (J_0) of the aligned lamellae.

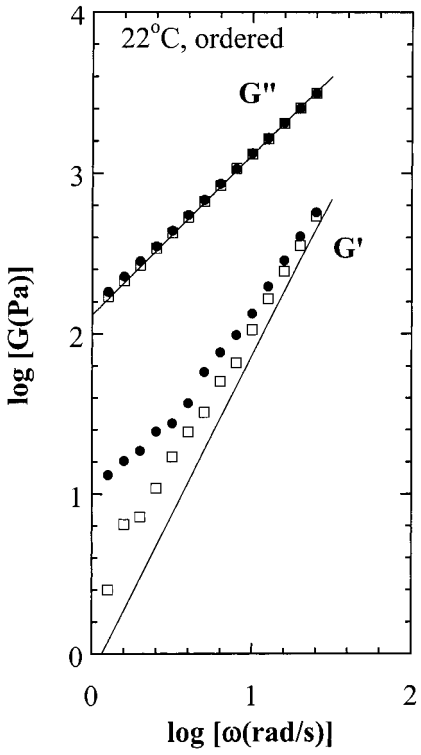

Figure 6. Frequency (ω) dependence of the storage (G') and loss (G'') moduli for ordered sample at 22 °C. Solid symbols: data from the sample with equilibrated defects. Open symbols: data from the best-aligned sample. Solid curves are theoretical fits using Rouse model (eqs 4 and 5) with τ_R as the only fitting parameter.

(H_{fast}). Thus, elimination of defects by shear alignment (reduction of H_{slow}) has little effect on G''. In contrast, the slow motion of defects, which is reflected in H_{slow}, dominates the low-frequency behavior of G' because H in the kernel for G' is magnified by the second power of τ (eq 2). Thus, G' at low frequencies decreases significantly during shear alignment.

The best-aligned perpendicular lamellae (not necessarily a single crystal), obtained after shearing for 660 min, exhibit terminal relaxation tails $G' \sim \omega^2$ and $G'' \sim \omega$ in our experimental window; see solid and dashed lines in Figure 5. The shearing conditions (thermal history, ω, strain amplitude, and time) required to obtain best alignment were identified by trying different conditions and noting the conditions that gave the lowest value of G' in the low-frequency regime. The zero-shear viscosity and recoverable compliance of perpendicular lamellae are obtained from the terminal relaxation tails as $\eta_0 = [G''/\omega]_{\omega\to 0} = 134 \pm 2$ Pa s and $J_0 = [G'/(G''^2)]_{\omega\to 0} = (7.2 \pm 1.1) \times 10^{-5}$ Pa^{-1}. The average relaxation time of the lamellae τ_0 is given by $J_0\eta_0 = 1.0 \times 10^{-2}$ s. In the absence of defects, this corresponds to the longest relaxation time of the perpendicular lamellae. Our objective was to access low-frequency behavior. The value of τ_0 of our system confirms that we have met our objective. (Accessible ω is significantly lower than $1/\tau_0$.)

The best-aligned state is not stable under quiescent conditions. After shear-aligning the sample for 660 min, we turned the motor off and waited for 120 min. We then measured G' and G'' of our ordered sample, and the results are shown in Figure 5 (t = 780 min data). The G'' data before and after turning off the motor are virtually identical due to the insensitivity of G'' to H_{slow}. In contrast, G' at low frequencies (ω < 1 rad/s) increases significantly under quiescent conditions (Figure 5). It is thus evident that the defects in our lamellar system are created spontaneously, and this leads to an increase in H_{slow}. This implies that the activation energy for defect formation in our sample is comparable to the thermal energy.[10]

It is evident that stable, defect-free SI[34−34]/DOP lamellae are unattainable. However, we found that the state represented by the filled circles in Figure 5 was stable on experimental time scales (ca. 1400 min). This state was obtained with a variety of shear and thermal histories provided that the alignment protocol was executed for more than 420 min. This fact suggests that the equilibrium defect density is achieved if we do not perturb our sample for 120 min or more after shear alignment. The remainder of the rheological characterization of the ordered state is limited to this stable, shear-aligned system having the equilibrium defect density.

This stable, shear-aligned system was cooled to 20 °C, and viscoelastic measurements were made as a function of increasing temperature. Typical results are shown in Figure 6 where the G' and G'' data obtained in the ordered state at 22 °C are plotted against the frequency ω (filled symbols). Also shown in Figure 6 are the G' and G'' data obtained from the best-aligned sample (open symbols). In the low-ω regime, G'' data obtained from the sample with best-aligned lamellae and the sample with equilibrated defects are almost identical. G'' is not significantly affected by the presence of equilibrated defects because of its insensitivity to weak but slow relaxation modes. The presence of defects is

clearly seen in the G' data (Figure 6) due to its sensitivity to these slow modes.

Let us now examine the fast relaxation modes due to motion of the copolymer chains. The chains in our SI/DOP solution are rather concentrated (hydrodynamic interactions are screened) but barely entangled; $\phi M \sim 22 \times 10^3$ g/mol ($\phi \approx 0.32$ is the polymer volume fraction) is comparable to the characteristic molecular weight for entanglement of PS and PI, $M_c = 36 \times 10^3$ g/mol (for PS), and $M_c = 10 \times 10^3$ g/mol (for PI).[41] For unentangled homopolymers at such large ϕ, the molecular relaxation process is well described by the Rouse model.[41] We thus use the Rouse model to describe the molecular relaxation of our SI copolymer chains.

$$G'_{\text{Rouse}}(\omega) = \sum_i \nu_i k_B T \left\{ \sum_{p \geq 1} \frac{\omega^2 \{\tau_{R,i}/p^2\}^2}{1 + \omega^2 \{\tau_{R,i}/p^2\}^2} \right\} \quad (4)$$

$$G''_{\text{Rouse}}(\omega) = \sum_i \nu_i k_B T \left\{ \sum_{p \geq 1} \frac{\omega \{\tau_{R,i}/p^2\}}{1 + \omega^2 \{\tau_{R,i}/p^2\}^2} \right\} \quad (5)$$

where k_B is the Boltzmann constant and T is the absolute temperature. In eqs 4 and 5, we have accounted for the polydispersity of the chains. We decomposed the GPC trace of our sample into 20 fractions and evaluated the number density ν_i and molecular weight M_i of the ith fraction. The longest relaxation time of the ith fraction is given by $\tau_{R,i} = \tau_R M_i^2/M_w^2$ where τ_R is the longest relaxation time of the copolymer chain with the weight-averaged molecular weight ($M_w = 68$ kg/mol). The ν_i and $\tau_{R,i}$ values thus determined were used to compute G'_{Rouse} and G''_{Rouse}, using the $p = 1-100$ terms in the summations in eqs 4 and 5. (For our sample, the effect of polydispersity was not significant: the difference between the monodisperse and polydisperse values of G'_{Rouse} and G''_{Rouse} were less than 15% at all frequencies. For completeness, however, we have included polydispersity in our calculations.)

The curves in Figure 6 represent calculations of G'_{Rouse} and G''_{Rouse} using eqs 4 and 5. The value of τ_R, the only unknown parameter in eqs 4 and 5, was chosen such that the calculated G''_{Rouse} in the high-frequency regime ($\omega > 30$ rad/s) was in agreement with the measured G'' data. With this choice of τ_R, the G' and G'' data of the best-aligned sample are in reasonable agreement with the Rouse model over the entire ω range (Figure 6). This result confirms that chain relaxation, which we have characterized by the Rouse model, dominates the low-frequency response of aligned lamellae. There are no significant additional slow relaxation modes due to the organization of the chains into lamellae. (The small discrepancy between the data and G'_{Rouse} seen in Figure 6 is probably due to the presence of a finite concentration of defects.)

We used the methodology described in the previous paragraph to analyze all of the data in the ordered state with equilibrated defects (temperature ≤ 28 °C). Typical results are shown in Figure 7, where we show data obtained from the sample equilibrated at 26 °C along with the Rouse predictions. Note the near quantitative agreement between the Rouse model and the experimental data over the entire frequency window for G'' and restricted agreement at high frequencies for G' (where the contribution of equilibrated defects to stress is unimportant). Similar agreement was observed at other temperatures in the ordered state.

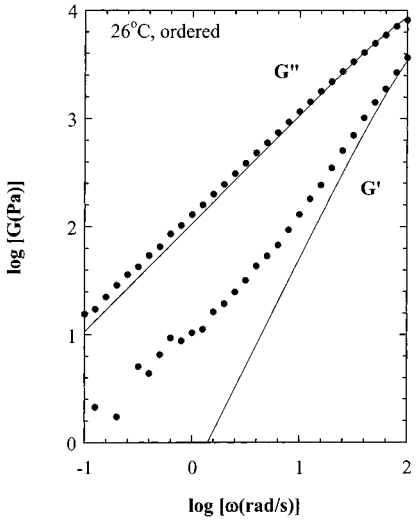

Figure 7. Frequency (ω) dependence of the storage (G') and loss (G'') moduli of the sample with equilibrated defects at 26 °C. Solid curves are theoretical fits using Rouse model (eqs 4 and 5) with τ_R as the only fitting parameter.

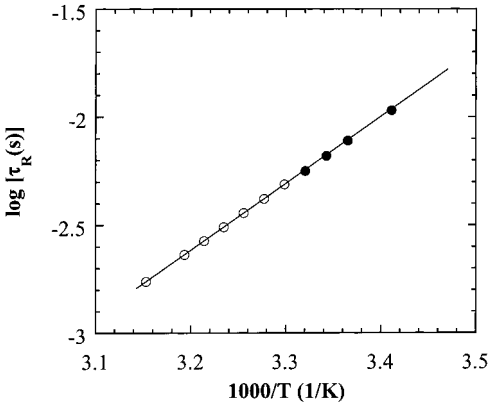

Figure 8. Temperature dependence of the chain relaxation time τ_R. Solid symbols show data from the shear-aligned lamellae. The line is the least-squares Arrhenius fit through the data from the shear-aligned lamellae. The open symbols represent extrapolated estimates of chain relaxation time τ_R in the disordered state.

The agreement between the Rouse model and data (for both best aligned and equilibrated systems) may be due to the fact that the copolymer chains are extremely mobile, and there is rapid exchange of chains between neighboring lamellae. This is not surprising because our ordered phase is in the vicinity of the order−disorder transition, and such motion is essential at equilibrium. However, the modulus for tethered Rouse chains (described by eqs 4 and 5 with the summation of p taken only for the odd modes[56]) is not significantly different from the modulus of untethered Rouse chains (eqs 4 and 5) at high frequencies ($\omega > 10$ s^{-1}). Further studies are required to determine the extent of tethering of block copolymer junctions between microstructures.

The Rouse fit to the rheological data in the ordered state described above enables determination of the temperature dependence of τ_R. In Figure 8 we plot τ_R vs $1/T$ (filled symbols). It is evident that τ_R obeys the Arrhenius relationship represented by the solid line in Figure 8; $\tau_R \sim \exp(E_a/RT)$ with the activation energy

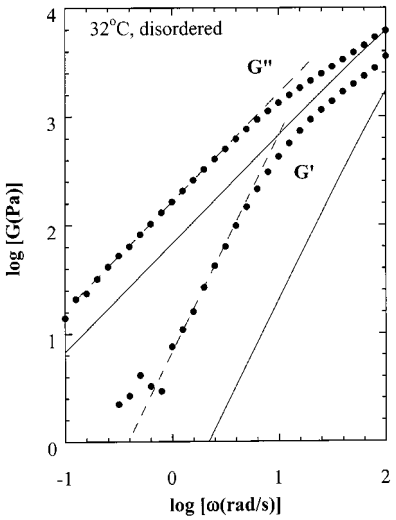

Figure 9. Frequency (ω) dependence of the storage (G') and loss (G'') moduli from the disordered sample at 32 °C. Solid lines are calculated using Rouse model and the relaxation time of individual chains at this temperature. Dashed lines were used to evaluate zero shear viscosity (η_0) and recoverable compliance (J_0) of the disordered fluid.

$E_a = 59$ kJ mol^{-1}. Extrapolating τ_R to higher T (between 30 and 44 °C), we estimated the chain relaxation time in the disordered state (unfilled circles in Figure 8).[57]

In the disordered state (temperature ≥ 30 °C), the SI/DOP system exhibited terminal behavior in our experimental window. Typical results are shown in Figure 9 (for the system at 32 °C). The solid curves indicate the Rouse moduli with τ_R from Figure 8. We see large deviations between the Rouse moduli and the experimental data. The magnitude of G'' at the highest frequency agrees well with the model, indicating that the high-frequency (or small length scale) dynamics are not very different from that expected by extrapolation of the data from the ordered state. However, the low-frequency G''_{Rouse} curves are well below the experimental data (Figure 9). Large differences between G'_{Rouse} and experiments are noted over the entire frequency window. It is obvious from Figure 9 that adjusting τ_R, which amounts to a simultaneous horizontal shift of the solid curves in Figure 9, will not lead to better agreement with experimental results. This is in stark contrast with the data obtained in the ordered state (Figures 6 and 7) where a single adjustable parameter τ_R resulted in good agreement between the Rouse model and experiment, particularly at high frequencies. Because the measured G' in the disordered state is significantly above that expected for chain relaxation, we conclude that these data are dominated by slow relaxation modes (H_{slow}). The presence of concentration fluctuations in disordered block copolymers near the order−disorder transition and their effect on rheology is well established in the literature.[19,53] We thus attribute the slow modes observed in the disordered state to concentration fluctuations.

The lack of agreement between the Rouse model and data evident in Figure 9 is seen in our sample at all temperatures (32−40 °C) above the order−disorder transition. However, since terminal behavior was observed in our experimental ω window, η_0 and J_0 could be rigorously determined (see dashed lines in Figure 9). At 32 °C, $\eta_0 = [G''/\omega]_{\omega\to 0} = 164 \pm 1$ Pa s and $J_0 = [G'/(G''^2)]_{\omega\to 0} = (2.5 \pm 0.3) \times 10^{-4}$ Pa^{-1}. Thus, while measuring η_0 and J_0 of the disordered phase is straightforward, interpreting the results is not straightforward. In contrast, the experimental determination of η_0 and J_0 of the aligned ordered phase is complicated by the presence of defects, but the interpretation of these data is straightforward due to agreement with the Rouse model.

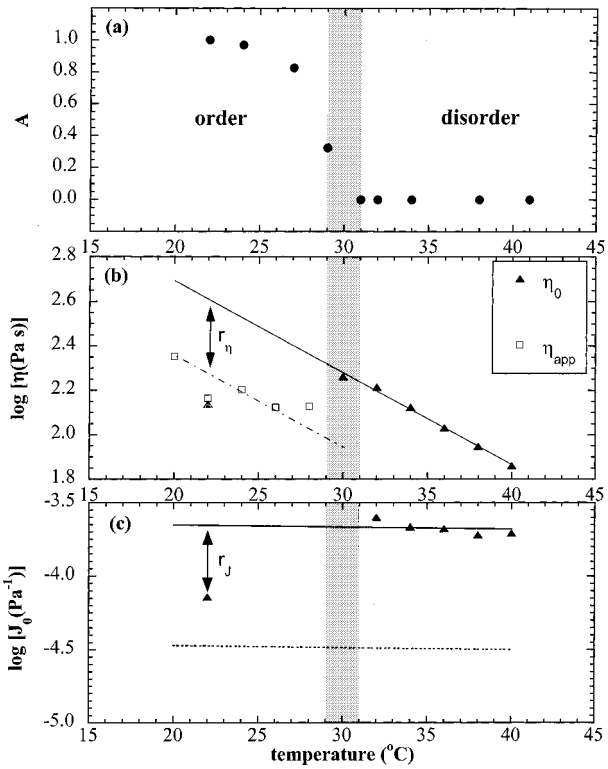

Figure 10. Temperature dependence of key structural and rheological features: (a) relative order parameter, A; (b) viscosity, η; (c) recoverable compliance, J. The η_0 and J_0 values at 22 °C (filled triangles) were obtained for the best-aligned system. r_η and r_J represent the changes in log of the viscosity and compliance, respectively, due to order formation. The dashed line in (c) is J_{Rouse}.

Discussion of Optical and Rheological Results

The structure−property relationships of the aligned lamellae in SI[34−34]/DOP solutions are depicted in Figure 10. The temperature dependence of the order parameter A, obtained from the birefringence experiments, is given in Figure 10a. It is evident that A decreases rapidly as T_{ODT} (30 °C) is approached. This is consistent with the fact that the order-to-disorder transition of block copolymer lamellae is a weakly first-order phase transition.[51,52]

The lamellae with equilibrated defect density did not exhibit terminal behavior (Figure 6): G' was not proportional to ω^2 due to defect-related slow modes. However, we argued that the slow relaxation intensity (H_{slow}) is rather small, and it has little influence on G''. Thus, we estimate the apparent viscosity η_{app} from the low-frequency G'' data by application of the relationship: $\eta_{app} = [G''/\omega]_{\omega\to 0}$. In Figure 10b, we show the temperature dependence of the zero-shear viscosity η_0 and the apparent viscosity η_{app}. Hereafter, we use the symbol η to refer collectively to η_0 and η_{app}. The exponential increase in viscosity η with decreasing temperature, observed in Figure 10b in the disordered state, is characteristic of fluids well above the glass transition temperature.[41] This trend reverses dramatically at the

order−disorder transition. The viscosity η exhibits nonmonotonic temperature dependence in the ordered state, indicating the interplay of two or more factors. One factor is the usual increase in molecular friction with decreasing temperature. The other factors must be related to the organization of the block copolymer chains into layers and the presence of concentration fluctuations in the disordered state. The temperature dependence of η_{app} in the ordered state well removed from the order−disorder transition parallels that of η_0 in the disordered state (dashed line in Figure 10b). We thus estimate the change in viscosity due to lamellar organization, $r_\eta = \log(\eta_{ord}/\eta_{disord}) = -0.5$, where η_{disord} and η_{ord} are the viscosities of the (metastable) disordered and ordered states at the same T, respectively (see Figure 10b for a graphical definition). The negative sign of r_η signifies a reduction of the viscosity upon ordering.

We take the calculated Rouse modulus G''_{Rouse} to be G''_{chain}, the loss modulus associated with the relaxation of individual chains. From this G''_{Rouse}, the contribution of this relaxation process to the zero-shear viscosity is estimated as $\eta_{chain} = [G''_{Rouse}/\omega]_{\omega\to 0}$. As noted from Figure 10b, this η_{chain} (obtained by extrapolating dashed line into the disordered state) is about a half of the measured η_0 in the disordered state. This implies that the chain relaxation and concentration fluctuations make roughly equal contributions to the measured η_0 in the disordered state. The unexpected decrease in viscosity with decreasing temperature (Figure 10b) thus reflects the suppression of concentration fluctuations in the ordered state.

Even though our explanation for the reduction of viscosity is reasonable, a detailed understanding of the viscoelastic changes that occur near the order−disorder transition is not possible due to the lack of knowledge of the local friction in the ordered and disordered states. This lack of knowledge forced us to obtain τ_R by fitting the rheological data (G''). It is therefore important to examine a friction-independent quantity, the steady-state compliance J_0. J_0 is a measure of the reciprocal of the terminal relaxation intensity, and it becomes large on broadening of the viscoelastic mode distribution.[41,53] In Figure 10c we show the temperature dependence of J_0. We have only one data point in the ordered state because J_0 could only be obtained from the best-aligned lamellae. The change in compliance due to lamellar organization is quantified by $r_J = \log(J_{ord}/J_{disord}) = -0.5$ where J_{disord} and J_{ord} are the compliances of the (metastable) disordered and ordered states at the same T, respectively (see Figure 10c for a graphical definition). The negative sign of r_J signifies a reduction of the compliance upon ordering.

The compliance according to the Rouse model can be readily calculated; $J_{Rouse} \approx 2M_w(M_w/M_n)^3/(5cRT)$, where c is the polymer concentration in mass/volume, R is the gas constant, and the $(M_w/M_n)^3$ factor accounts for mode broadening due to the distribution of molecular weights. Note that J_{Rouse} can be calculated without resorting to the rheological data. The results of this calculation are indicated by the dashed line in Figure 10c. It is evident in Figure 10c that J_0 of the disordered state is about an order of magnitude larger than J_{Rouse}. In contrast, the J_0 of the best-aligned lamellae is within a factor of 2 of J_{Rouse}. This level of disagreement between the J_0 values obtained from experiments, and the Rouse model is also seen in much simpler systems such as unentangled homopolymer melts.[41] Further, the fast relaxation spectrum of the best-aligned sample is well described by the Rouse model; see curves in Figure 6. Thus, the increased elasticity of the disordered phase must arise from concentration fluctuations, which may be viewed as temporary aggregates.

Table 2. Literature Values of Exponents of G' vs ω and G'' vs ω, $\nu_{G'}$ and $\nu_{G''}$, in the Low Frequency Limit[59]

		parallel		perpendicular	
ref	polymer	$\nu_{G'}$	$\nu_{G''}$	$\nu_{G'}$	$\nu_{G''}$
19	PEP−PEE(30−25)	1.9	1.0		
20	PEP−PEE(45−36)	0.8	0.8	0.8	0.9
21	SI(10−10)	1.3	1.0	0.7	1.0
26	SI(12.5−9.5)	0.6	0.7	1.2	1.0
27	SI(11−10)	0.6	0.6	1.2	1.0

Finally, we address the nonmonotonic time dependence of the peak stress (σ_{peak}) during order formation under shear flow shown in Figure 4. During most of the experiment (10 min < t < 1000 min) σ_{peak} decreases with time. This makes sense because the aligned ordered phase that is being formed during the experiment is less viscous and less compliant than the disordered phase. The increase of σ_{peak} during $t \le 10$ min can be therefore attributed to the formation of a supercooled disordered phase, which has a higher viscosity and compliance than the ordered state. The viscosity of the supercooled disordered phase, based on the σ_{peak} value at $t = 10$ min in Figure 4, is estimated to be 320 Pa s (σ_{peak}/ω; strain = 100%).[58] The estimated viscosity of the supercooled disordered phase at 22 °C, based on the extrapolated solid line in Figure 10b, is 400 Pa s. The difference between these two estimates is well within the uncertainty of the extrapolation in Figure 10b. Thus, the peak in σ_{peak} in Figure 4 represents the rheological signature of the beginning of the disorder-to-order transition. It is evident that the rheological signature of the beginning of order formation (which is observed at $t = 10$ min) occurs well before the optical signature of the beginning of order formation (which is observed at $t = 80$ min). We cannot rule out the possibility of the growth of a small concentration of ordered grains (below the detection limit of our optical instrument) during 10 min $\le t \le$ 80 min.

Concluding Remarks

The organization of the copolymer chains into lamellae leads to a reduction in both compliance and viscosity, relative to the disordered state. The measured G' and G'' data of the best-aligned lamellae are consistent with the Rouse model. In addition, the measured compliance of the aligned lamellae is within a factor of 2 of the Rouse model (calculated with no adjustable parameters). Thus, molecular relaxation is the slowest relaxation mode in our best-aligned sample; no additional slow modes arise due to the organization of block copolymer chains into lamellae. In contrast, the rheology of weakly ordered lamellar systems formed by small molecules contain significant contributions due to lamellar fluctuations.[25,37,38]

In Table 2, we summarize the results of previous rheological studies of aligned block copolymer lamellae.[19−21,26,27] We fit power laws through the low-frequency G' and G'' data, and the resulting exponents $\nu_{G'}$ and $\nu_{G''}$ are reported in Table 2.[41,59] If G' and G'' exhibit nonterminal power law dependencies on ω in the $\omega \to 0$ limit, then the Kramers−Kronig relationship requires that $\nu_{G'} = \nu_{G''} < 1$, as is the case in systems

such as critical gels.[41,60] It is clear from examining Table 2 that some of the results are in (approximate) agreement with the Kramers−Kronig relationship while others are not. More importantly, none of the systems except parallel poly(ethylenepropylene)-*block*-poly(ethylethylene) copolymer (PEP−PEE) lamellae[19] exhibit terminal behavior.

Bates et al. conducted rheological measurements on the PEP−PEE system just after cooling from $T > T_{ODT}$ to $T < T_{ODT}$ before significant order had formed.[19] They then aligned the sample and measured its rheological properties. Both the metastable disordered state at $T < T_{ODT}$ and the aligned lamellae exhibited terminal behavior. Thus, η_0 and J_0 for both states can be evaluated. The r_η and r_J values for the PEP−PEE system are −0.3 and −1.1, respectively. The viscosity and compliance thus decrease upon alignment, as was the case with our SI/DOP system. This suggests that the reduction of viscosity and compliance upon ordering and aligning may be a general result; i.e., it applies to solutions and melts, entangled and unentangled systems, parallel and perpendicular alignment. Additional support for this statement is contained in ref 21 where it is reported that G'' of parallel SI lamellae is lower than that of the disordered state at the same reference temperature. It is likely that the lack of terminal behavior seen in Table 2 is attributable to imperfect alignment. More data on highly aligned systems are required before general conclusions regarding the low-frequency behavior of aligned lamellae are reached.

It is clear that reducing defect density is crucial for understanding the rheology of aligned block copolymer lamellae. More systematic rheological studies on defect-free system would be useful at this juncture. In our system, the spontaneous formation of defects under quiescent conditions severely limited our characterization of the ordered state. Identifying block copolymer systems with stable defect-free states deserves further attention.

Acknowledgment. H.H., J.H.L., N.P.B., and B.A.G. gratefully acknowledge financial support of the National Science Foundation (DMR-9901951, DMR-9975592). H.W. acknowledges support from Japan Chemical Innovation Institute (through the Doi Project).

References and Notes

(1) Keller, A.; Pedemonte, E.; Willmouth, F. M. *Nature* **1970**, *225*, 538.
(2) Folkes, M. J.; Keller, A. *Polymer* **1971**, *12*, 222.
(3) Chung, C. I.; Gale, J. C. *J. Polym. Sci., Polym. Phys. Ed.* **1976**, *14*, 1149.
(4) Hadziioannou, G.; Mathis, A.; Skoulios, A. *Colloid Polym. Sci.* **1979**, *257*, 136.
(5) Ohta, T.; Kawasaki, K. *Macromolecules* **1986**, *19*, 2621.
(6) Fredrickson, G. H. *J. Chem. Phys.* **1986**, *85*, 5306.
(7) Fredrickson, G. H.; Larson, R. G. *J. Chem. Phys.* **1987**, *86*, 1553.
(8) Onuki, A. *J. Chem. Phys.* **1987**, *87*, 3692.
(9) Kawasaki, K.; Onuki, A. *Phys. Rev. A* **1990**, *42*, 3664.
(10) Amundson, K.; Helfand, E. *Macromolecules* **1993**, *26*, 1324.
(11) Ohta, T.; Enomoto, Y.; Harden, J. L.; Doi, M. *Macromolecules* **1993**, *26*, 4928.
(12) Wang, Z. G. *J. Chem. Phys.* **1994**, *100*, 2298.
(13) Williams, D. R. M.; Mackintosh, F. C. *Macromolecules* **1994**, *27*, 7677.
(14) Kodama, H.; Doi, M. *Macromolecules* **1996**, *29*, 2652.
(15) Cates, M. E.; Milner, S. T. *Phys. Rev. Lett.* **1989**, *62*, 1856.
(16) Doi, M.; Ohta, T. *J. Chem. Phys.* **1991**, *95*, 1242.
(17) Fredrickson, G. H. *J. Rheol.* **1994**, *38*, 1045.
(18) Goulian, M.; Milner, S. T. *Phys. Rev. Lett.* **1995**, *74*, 1775.
(19) Bates, F. S.; Rosedale, J. H.; Fredrickson, G. H. *J. Chem. Phys.* **1990**, *92*, 6255.
(20) Koppi, K. A.; Tirrell, M.; Bates, F. S.; Almdal, K.; Colby, R. H. *J. Phys. II* **1992**, *2*, 1941.
(21) Gupta, V. K.; Krishnamoorti, R.; Kornfield, J. A.; Smith, S. D. *Macromolecules* **1995**, *28*, 4464.
(22) Gupta, V. K.; Krishnamoorti, R.; Kornfield, J. A.; Smith, S. D.; Satowski, M. M.; Grothaus, J. T. *Macromolecules* **1996**, *29*, 875.
(23) Gupta, V. K.; Krishnamoorti, R.; Kornfield, J. A.; Smith, S. D. *Macromolecules* **1996**, *29*, 1359.
(24) Chen, Z. R.; Issaian, A. M.; Kornfield, J. A.; Smith, S. D.; Grothaus, J. T.; Satowski, M. M. *Macromolecules* **1997**, *30*, 7114.
(25) Larson, R. G.; Winey, K. I.; Patel, S. S.; Watanabe, H.; Bruinsma, R. *Rheol. Acta* **1993**, *32*, 245.
(26) Patel, S. S.; Larson, R. G.; Winey, K. I.; Watanabe, H. *Macromolecules* **1995**, *28*, 4313.
(27) Pinheiro, B. S.; Winey, K. I. *Macromolecules* **1998**, *31*, 4447.
(28) Zhang, Y.; Wiesner, U. *J. Chem. Phys.* **1995**, *103*, 4784.
(29) Balsara, N. P.; Hammouda, B. *Phys. Rev. Lett.* **1994**, *72*, 360.
(30) Balsara, N. P.; Hammouda, B.; Kesani, P.; Jonnalagadda, S. V.; Straty, G. C. *Macromolecules* **1994**, *27*, 2556.
(31) Wang, H.; Kesani, P.; Balsara, N. P.; Hammouda, B. *Macromolecules* **1997**, *30*, 982.
(32) Garetz, B. A.; Balsara, N. P.; Dai, H. J.; Wang, Z.; Newstein, M. C.; Majumdar, B. *Macromolecules* **1996**, *29*, 4675.
(33) de Gennes, P. G.; Prost, J. *The Physics of Liquid Crystals*; Oxford University Press: New York, 1993.
(34) Martin, P. C.; Parodi, O.; Pershan, P. S. *Phys. Rev. A* **1971**, *6*, 2401.
(35) Cagnon, M.; Durand, G. *Phys. Rev. Lett.* **1980**, *45*, 1418.
(36) Milner, S. T.; Martin, P. C. *Phys. Rev. Lett.* **1986**, *56*, 77.
(37) Bruinsma, R.; Rabin, Y. *Phys. Rev. A* **1992**, *45*, 994.
(38) Bruinsma, R. F.; Safinya, C. R. *Phys. Rev. A* **1991**, *43*, 5377.
(39) Jamieson, A. M.; Gu, D.; Chen, F. L.; Smith, S. *Prog. Polym. Sci.* **1996** *21*, 981.
(40) Graessley, W. W. *Physical Properties of Polymers*; American Chemical Society: Washington, DC, 1993; Chapter 3.
(41) Ferry, J. D. *Viscoelastic Properties of Polymers*; Wiley: New York, 1980.
(42) Lin, C. C.; Jonnalagadda, S. V.; Kesani, P. K.; Dai, H. J.; Balsara, N. P. *Macromolecules* **1994**, *27*, 7769.
(43) Balsara, N. P.; Perahia, D.; Safinya, C. R.; Tirrell, M.; Lodge, T. P. *Macromolecules* **1992**, *25*, 3896.
(44) Bates, F. S.; Rosedale, J. H.; Bair, H. E.; Russell, T. P. *Macromolecules* **1989**, *22*, 2557.
(45) Wang, H.; Newstein, M. C.; Chang, M. Y.; Balsara, N. P.; Garetz, B. A. *Macromolecules* **2000**, *33*, 3719.
(46) Lodge, T. P.; Fredrickson, G. H. *Macromolecules* **1992**, *25*, 5643.
(47) Balsara, N. P.; Garetz, B. A.; Dai, H. J. *Macromolecules* **1992**, *25*, 6072.
(48) Dai, H. J.; Balsara, N. P.; Garetz, B. A.; Newstein, M. C. *Phys. Rev. Lett.* **1996**, *77*, 3677.
(49) Wang, H.; Newstein, M. C.; Krishnan, A.; Balsara, N. P.; Garetz, B. A.; Hammouda, B.; Krishnamoorti, R. *Macromolecules* **1999**, *32*, 3695.
(50) Born, M.; Wolf, E. *Principles of Optics*; Pergamon: New York, 1975.
(51) Leibler, L. *Macromolecules* **1980**, *13*, 1602.
(52) Fredrickson, G. H.; Helfand, E. *J. Chem. Phys.* **1987**, *87*, 697.
(53) Watanabe, H. Rheology of Multiphase Polymeric Systems. In Araki, T.; Tran-Cong, Q.; Shibayama, M. *Structure and Properties of Multiphase Polymeric Materials*; Marcel Dekker: New York, 1998; Chapter 9.
(54) Bates, F. S.; Koppi, K. A.; Tirrell, M.; Almdal, K.; Mortenson, K. *Macromolecules* **1994**, *27*, 5934.
(55) Almdal, K.; Mortenson, K.; Koppi, K. A.; Tirrell, M.; Bates, F. S. *J. Phys II* **1996**, *6*, 617.
(56) Graessley, W. W. *Adv. Polym. Sci.* **1982**, *47*, 67.
(57) The Williams−Landel−Ferry (WLF) equation can also be used to fit the τ_R vs T data at $T \leq 28$ °C. The values of τ_R in the disordered state ($T = 30-44$ °C) estimated from this fit differ from that obtained from the Arrhenius relationship by <50%. This minor difference does not affect the validity of our arguments.
(58) The value of viscosity computed here is a very rough estimate due to the large strain (100%) involved.

(59) In some cases, significantly lower exponents ($\nu_{G'}$ and $\nu_{G''}$) would be obtained if the lowest frequency data were included. As we show in this paper, the anomalies seen at very low frequencies are probably due to incomplete elimination of defects. Since we are interested in characterizing the flow of lamellae in the absence of defects, low-frequency tails with apparent exponents that are much smaller than the $\nu_{G'}$ and $\nu_{G''}$ values reported in Table 2 are ignored.

(60) Winter, H. H.; Mours, M. *Adv. Polym. Sci.* **1997**, *134*, 165.

MA0109929